

# Query-Based Adaptive Aggregation for Multi-Dataset Joint Training Toward Universal Visual Place Recognition

Jiuhong Xiao<sup>1</sup>, Yang Zhou<sup>1</sup>, Giuseppe Loianno<sup>1</sup>

<sup>1</sup>New York University

jx1190@nyu.edu, yz5794@nyu.edu, loiannog@nyu.edu

## Abstract

Deep learning methods for Visual Place Recognition (VPR) have advanced significantly, largely driven by large-scale datasets. However, most existing approaches are trained on a single dataset, which can introduce dataset-specific inductive biases and limit model generalization. While multi-dataset joint training offers a promising solution for developing universal VPR models, divergences among training datasets can saturate limited information capacity in feature aggregation layers, leading to suboptimal performance. To address these challenges, we propose Query-based Adaptive Aggregation (QAA), a novel feature aggregation technique that leverages learned queries as reference codebooks to effectively enhance information capacity without significant computational or parameter complexity. We show that computing the Cross-query Similarity (CS) between query-level image features and reference codebooks provides a simple yet effective way to generate robust descriptors. Our results demonstrate that QAA outperforms state-of-the-art models, achieving balanced generalization across diverse datasets while maintaining peak performance comparable to dataset-specific models. Ablation studies further explore QAA’s mechanisms and scalability. Visualizations reveal that the learned queries exhibit diverse attention patterns across datasets. Code will be publicly released.

## Introduction

Visual Place Recognition (VPR) (Schubert et al. 2024; Zafar et al. 2021; Berton et al. 2022) is a fundamental computer vision task that involves retrieving the top-K most similar images from a database of geo-referenced or pose-annotated images given a query image. Learning-based VPR methods (Arandjelovic et al. 2016; Ge et al. 2020; Berton et al. 2023; Berton, Masone, and Caputo 2022; Izquierdo and Civera 2024a,b; Ali-bey, Chaib-draa, and Giguère 2022, 2023; Lu et al. 2024; Ali-bey, Chaib-draa, and Giguère 2024; Tzachor et al. 2025; Xiao, Zhu, and Loianno 2025; Leyva-Vallina, Strisciuglio, and Petkov 2023; Trivigno et al. 2023) are widely applied in computer vision and robotics, particularly in tasks such as large-scale coarse-to-fine camera localization (Sarlin et al. 2019), loop closure in SLAM systems (Masone and Caputo 2021; Campos et al. 2021), and absolute localization in GPS-denied environments (Couturier and Akhloufi 2021; Xiao et al. 2023). However, outdoor VPR still faces challenges, including significant variations due to domain shifts (e.g., day-night variation),

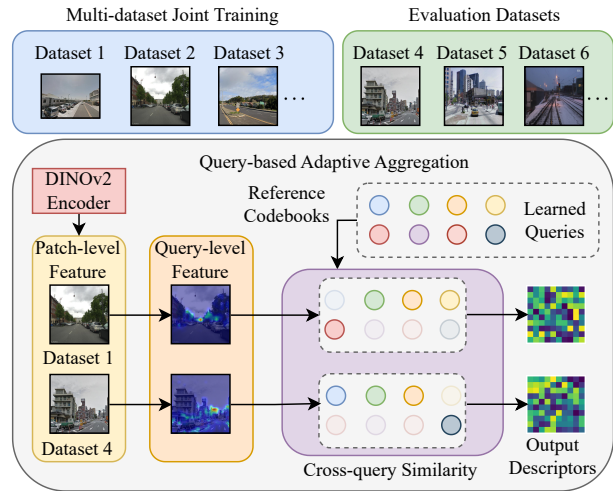


Figure 1: Query-based Adaptive Aggregation (QAA) for Multi-Dataset Joint Training toward Universal Visual Place Recognition (VPR). QAA calculates cross-query similarity matrices between query-level image features and reference codebooks—constructed by learned queries—for output descriptors, improving the information capacity of aggregation layers and enhancing cross-domain generalization.

changes in viewpoint (e.g., front-view vs. multi-view), occlusion by moving objects, and the absence of prominent landmarks. To address these challenges, researchers have developed several outdoor large-scale VPR datasets (Warburg et al. 2020; Berton, Masone, and Caputo 2022; Ali-bey, Chaib-draa, and Giguère 2022) to train robust models, each capturing different environmental conditions and scene characteristics. These datasets introduce specific biases influenced by factors such as camera viewpoint, domain, sampling density, and geographic diversity, outlined in Table 1.

Joint training across multiple VPR datasets (Izquierdo and Civera 2024a; Berton and Masone 2025; Liu et al. 2025) has emerged as a promising approach to achieving more robust and universally applicable outdoor VPR models. One pioneering example, SALAD Clique Mining (CM) (Izquierdo and Civera 2024a), introduced a clique-based grouping method to cluster densely sampled images from the MSLS

dataset (Warburg et al. 2020), facilitating joint training with the sparser GSV-Cities dataset (Ali-bey, Chaib-draa, and Giguère 2022). Our cross-dataset evaluations similarly indicate that models trained exclusively on single datasets become biased toward specific dataset characteristics, resulting in limited generalization capability. Conversely, joint training across multiple diverse datasets consistently yields superior performance in a broad range of benchmarks. Nonetheless, our results also show that the baseline aggregation protocol proposed in (Izquierdo and Civera 2024b) occasionally underperforms relative to dataset-specific models, likely due to significant training dataset divergence and limited information capacity in feature aggregation layers.

To address these challenges, we introduce Query-based Adaptive Aggregation (QAA) (Fig. 1), a novel feature aggregation method aimed at enhancing multi-dataset joint training performance. QAA employs learned queries as reference codebooks to efficiently expand memory within aggregation layers, thereby increasing information capacity and maintaining strong performance even with low-dimensional descriptors. This approach strengthens cross-domain generalization while preserving peak performance comparable to dataset-specific models. By utilizing the cross-query similarity matrix between query-level image features and the independent reference codebook, QAA effectively models robust geographic descriptors that capture the relative spatial relationships between images. The adaptive learned queries enable the generation of diverse feature representations across datasets while introducing minimal computational and parameter overhead. The main contributions are as follows:

- We propose the **Query-based Adaptive Aggregation (QAA)** approach that utilizes learned queries as the independent reference codebook for aggregation. QAA demonstrates its strengths in capturing the global context for query-level image features and reference codebooks, handling scalable queries without increasing output descriptor dimensions, and maintaining minimal computational and parameter overhead.
- We introduce **Cross-query Similarity (CS)**, a simple yet effective aggregation paradigm that constructs similarity matrices between image features and reference codebooks to generate robust geographic descriptors. We analyze its information capacity through coding rate (Ma et al. 2007; Yu et al. 2020), providing insights into its superior performance.
- Extensive evaluations demonstrate that QAA outperforms state-of-the-art VPR methods, achieving balanced generalization across diverse datasets and peak performance compared with models trained on specific datasets. Ablation studies and visualizations provide insight into the mechanism and scalability of QAA, demonstrating the enhanced information capacity of aggregation layers for better performance and diverse attention patterns in various datasets.

## Related Works

Learning-based VPR methods can be broadly categorized into one-stage (Arandjelovic et al. 2016; Ge et al. 2020;

Berton et al. 2023; Berton, Masone, and Caputo 2022; Izquierdo and Civera 2024a,b; Ali-bey, Chaib-draa, and Giguère 2022, 2023; Leyva-Vallina, Strisciuglio, and Petkov 2023) and two-stage approaches (Zhu et al. 2023; Wang et al. 2022; Lu et al. 2024; Tzachor et al. 2025; Trivigno et al. 2023). One-stage methods typically employ a CNN (LeCun, Bengio, and Hinton 2015) or ViT (Dosovitskiy et al. 2021) model as the feature extractor, generating local feature maps, followed by a feature aggregation module to convert the 2D feature map into a 1D global descriptor. The query image descriptor is then compared against a database to identify the top-K similar images and retrieve their geo-referenced information. Two-stage methods, in contrast, re-rank these top-k candidates by further utilizing the 2D feature maps, achieving enhanced localization performances with higher computational costs. In VPR, the output dimensionality of descriptors plays a crucial role, with a linear impact on both memory usage and matching cost.

Score-based feature aggregation methods (Arandjelovic et al. 2016; Izquierdo and Civera 2024b), also known as cluster-based aggregation, compute global descriptors by weighting and summing patch-level image features based on predicted scores. For instance, NetVLAD (Arandjelovic et al. 2016) uses softmax scores to weight the distances between image features and cluster centroids. Similarly, SALAD (Izquierdo and Civera 2024b) weights patch features by scores normalized with the Sinkhorn optimal transport algorithm (Sinkhorn and Knopp 1967; Cuturi 2013). In contrast, our QAA method eliminates explicit score prediction. Instead, it generates robust descriptors by computing a cross-query similarity matrix between learned query-level image features and an independent reference codebook, achieving comparable or reduced dimensionality.

Recent VPR methods leverage foundational models like DINOv2 (Oquab et al. 2024) for better generalization. For example, AnyLoc (Keetha et al. 2023) leverages general-purpose representations from DINOv2, SelaVPR adds lightweight adapters to DINOv2, and EffoVPR uses DINOv2’s self-attention features for reranking. The most relevant work, BoQ (Ali-bey, Chaib-draa, and Giguère 2024), utilizes learned queries to project image features from a DINOv2 backbone. Unlike BoQ’s concatenation approach, which combines all learned query outputs and reduces dimensionality with linear layers, our QAA method computes cross-query similarity with independent reference codebooks. This approach prevents the output dimension from increasing with the number of queries, enabling scalable query use with a fixed output size.

## Methodology

### Framework Overview

We present the training framework (Fig. 2) for multi-dataset training. We denote  $\mathcal{D} = \{D_1, D_2, \dots, D_n\}$  as training datasets, where  $n$  is the number of datasets. From each dataset, we sample  $k$  places, with each place consisting of  $m$  images. The concatenated batch from all datasets is represented as  $\mathcal{B} = \{B_1, B_2, \dots, B_n\}$ , where  $\mathcal{B}$  contains  $n \times k \times m$  images in total as the input image batch.

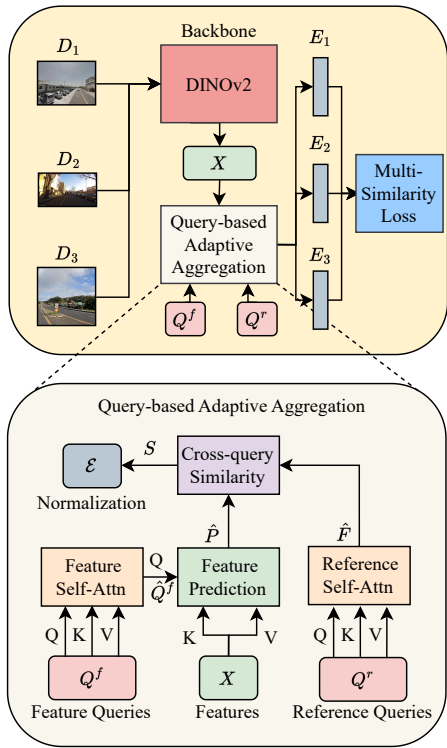


Figure 2: The training framework (top) and Query-Based Adaptive Aggregation (QAA) architecture (bottom)

We use DINOv2-B/14 (Oquab et al. 2024) as the backbone to balance performance and latency. The input has dimensions  $N \times C \times H \times W$ , where  $N = n \times k \times m$  represents the number of images per batch, and  $C, H,$  and  $W$  are the image channels, height, and width. The output includes a feature map  $X$  of size  $N \times P \times C_o$ , with  $P = \frac{H}{14} \times \frac{W}{14}$  and  $C_o$  as the output feature map channels. We then employ the Query-based Adaptive Aggregation (QAA) method for feature aggregation. The final outputs  $\mathcal{E}$  are descriptors of size  $N \times C_d$ , where  $C_d$  represents the output descriptor dimension. This output can be decomposed as  $\mathcal{E} = \{E_1, E_2, \dots, E_n\}$  for each dataset. The overall framework design allows the flexibility to incorporate additional datasets for joint training.

We employ Multi-Similarity (MS) Loss (Wang et al. 2019; Ali-bey, Chaib-draa, and Giguère 2022) to train the final blocks of the DINOv2 model along with the QAA module. Images from the same place are grouped and treated as positive examples, while images from different places (groups) serve as negative samples.

### Query-based Adaptive Aggregation (QAA)

Figure 2 illustrates the Query-based Adaptive Aggregation (QAA) approach. We define the learnable parameters—reference queries  $Q^r$  and feature queries  $Q^f$ —with dimensions  $N_q \times C_r$  and  $N_q \times C_o$ , respectively, where  $N_q$  represents the number of queries,  $C_r$  represents the number of channels for  $Q^r$ . These queries are learned via backprop-

agation during training, without test-time adaptation.

**Query-Level Image Features.** To generate query-level image features  $\hat{P}$ , QAA employs two modules: 1) a *Feature Self-Attention (Feature Self-Attn)* mechanism, utilizing a Multi-Head Attention (MHA) module (Vaswani et al. 2017), and 2) a *Feature Prediction* module, which integrates an MHA module with a projection layer to reduce the channel dimension to  $C_f$ , where  $C_f$  represents the number of channels for  $\hat{P}$ . This process is defined as:

$$\hat{Q}^f = Q^f + \text{Feature-Self-Attn}(Q^f, Q^f, Q^f), \quad (1)$$

$$\hat{P} = \text{Feature-Prediction}(\hat{Q}^f, X, X), \quad (2)$$

where  $\hat{P}$  denotes the query-level image features with dimensions  $N_q \times C_f$  (omitting the batch dimension for simplicity) and  $\hat{Q}^f$  denotes the self-attention-refined version of  $Q^f$ . The patch-level image feature  $X$  serves as the key and value in the feature prediction module. The inclusion of the self-attention module, inspired by (Ali-bey, Chaib-draa, and Giguère 2024), minimizes the need for substantial modifications to  $Q^f$ , thereby enhancing training stability and accelerating convergence.  $\hat{Q}^f$  can be cached after training.

**Independent Reference Codebook.** The reference codebook  $\hat{F}$  is derived from the reference queries  $Q^r$  using a *Reference Self-Attention (Ref-Self-Attn)* mechanism implemented with an MHA module:

$$\hat{F} = Q^r + \text{Ref-Self-Attn}(Q^r, Q^r, Q^r) \quad (3)$$

where  $\hat{F}$  represents the reference codebook with dimensions  $N_q \times C_r$ . Similar to  $\hat{Q}^f$ ,  $\hat{F}$  can be cached after training. By employing these learned queries as the reference codebooks for feature aggregation, QAA enhances the information capacity of the aggregation layers and transforms the predicted features—whose dimensionality scales with the query count—into fixed-dimensional descriptors, ensuring scalability regardless of the input complexity.

**Cross-query Similarity.** The Cross-query Similarity (CS) matrix  $S$ , of dimensions  $C_r \times C_f$ , quantifies the similarity between image features and the reference codebook. It is computed through matrix multiplication of  $\hat{P}$  and  $\hat{F}$ :

$$S = \hat{F}^\top \hat{P}, \quad (4)$$

where  $S$  represents the pairwise similarity matrix between  $\hat{F}$  and  $\hat{P}$  along the query dimension of  $N_q$ , justifying the term *Cross-query Similarity*. Notably, this mechanism is similar to the similarity computation between keys and queries in the attention mechanism (Vaswani et al. 2017). However, a key distinction is that while attention computes similarity along the channel dimension, QAA performs similarity computation along the query dimension. Equation 4 fundamentally computes the cross-correlation matrix between query-level image features and codebooks, effectively capturing second-order statistics along the query dimension.

The final descriptor  $\mathcal{E}$  is obtained by applying intra-L2 normalization on  $S$  along the  $C_r$  dimension (Arandjelovic et al. 2016), followed by a global L2 normalization of the entire vector. The output descriptor dimension  $C_d$  is given

Table 1: Overview of large-scale VPR datasets for joint training. \* Sampling density refers to the spacing between sampled locations, with each location potentially containing multiple images.

Datasets	GSV-Cities (Ali-bey, Chaib-draa, and Giguère 2022)	MSLS (Warburg et al. 2020)	SF-XL (Berton, Masone, and Caputo 2022)
Viewpoint	multi-view	front-view	multi-view
Domain	urban	mostly urban	mostly urban
Sampling Density*	sparse	dense	dense
Number of Cities	multiple	multiple	single
Season Variation	✓	✓	✓
Day-night Change		✓	
Weather Conditions	✓	✓	✓

by  $C_r \times C_f$ . During inference, the aggregation process involves only the computations from Equations 2 and 4, along with the final normalization. This ensures that QAA maintains minimal computational and parameter complexity.

Our intuition behind the CS paradigm is to preserve the information capacity of  $\hat{P}$ . Unlike score-based paradigms that compress the output space into the range  $[0, 1]$ , the CS paradigm avoids such projection, retaining more information for interaction with the reference codebook. To quantify the information retained in  $\hat{P}$ , we leverage the coding rate concept from information theory (Ma et al. 2007; Yu et al. 2020). The coding rate is computed as:

$$R(\hat{P}^\top, \epsilon) = \frac{1}{2} \log \det \left( I + \frac{C_f}{N_q \epsilon^2} \hat{P}^\top \hat{P} \right) \quad (5)$$

where  $R(\hat{P}^\top, \epsilon)$  represents the coding rate of the random variable  $\hat{p}$ , with finite samples given by  $\hat{P}^\top = [\hat{p}_1, \dots, \hat{p}_{N_q}]$ , having dimensions  $C_f \times N_q$  and a prescribed precision  $\epsilon$ , which is set to 0.001. This equation utilizes the covariance matrix  $\hat{P}^\top \hat{P}$  to quantify the information capacity of  $\hat{P}$ . Our coding rate analysis demonstrates that the coding rate of  $\hat{P}$  in the CS paradigm exceeds that of OT and Softmax, despite sharing the same dimensionality. This result validates the superior information capacity of CS. This enhanced capacity enables CS to generate more informative descriptors, ultimately leading to improved performance.

CS aggregation paradigm represents a significant advancement in retrieval-based VPR, as it demonstrates—for the first time—that informative geographic descriptors can be formulated directly from the similarity matrix between query-level image features and an independent reference codebook. This eliminates the need for explicit score prediction techniques (Arandjelovic et al. 2016; Izquierdo and Civera 2024b) or implicit linear projection. Therefore, CS aggregation enhances the interpretability of descriptor generation in retrieval-based VPR.

## Experimental Setup

**Datasets.** For multi-dataset joint training, we utilize GSV-Cities (Ali-bey, Chaib-draa, and Giguère 2022) with sparse place sampling, MSLS (Warburg et al. 2020) incorporating place cluster information, and SF-XL (Berton, Masone, and Caputo 2022), which is grouped by location and orientation.

These large-scale datasets encompass a wide range of variations essential for outdoor VPR, as outlined in Table 1.

For evaluation, we incorporate a wide range of VPR datasets. The AmsterTime dataset (Yildiz et al. 2022) matches historical grayscale images with current RGB images, testing robustness to long-term temporal changes. The Eynsham dataset (Cummins and Newman 2009) focuses on grayscale images for VPR. Pittsburgh (Torii et al. 2013), Tokyo24/7 (Torii et al. 2015), and SF-XL (Berton, Masone, and Caputo 2022) datasets utilize Google Street View as the source of database images and primarily assess viewpoint variations. MSLS (Warburg et al. 2020) collects images from a forward-facing car-mounted camera. Nordland\*\* (Sünderhauf, Neubert, and Protzel 2013) examines seasonal changes between summer and winter conditions, using a 10-frame threshold for positive samples, while its variant, Nordland\* (Zaffar et al. 2021), employs a 1-frame threshold, demanding higher accuracy. The SPED dataset (Chen et al. 2017) captures seasonal and day-night variations using surveillance footage. SVOX (Berton et al. 2021) poses varying illumination and weather conditions.

**Evaluation Metrics.** We evaluate VPR performance using Recall@1 (R@1), focusing on the proportion of query samples with correct top-1 matches. Following prior works (Ali-bey, Chaib-draa, and Giguère 2024; Izquierdo and Civera 2024b), positive matches are defined using a 25 m distance threshold for most datasets, while frame-based thresholds are used for datasets like Nordland (Sünderhauf, Neubert, and Protzel 2013; Zaffar et al. 2021).

**Implementation details.** For multi-dataset joint training, we set  $k = 30$  and  $m = 4$  per dataset, resulting in a batch size of 90 places and 360 images. Training images are resized to  $224 \times 224$  and evaluation images to  $322 \times 322$ . We fine-tune the last two blocks of the DINOv2 model (Oquab et al. 2024) alongside the QAA module, selecting models based on MSLS val performance. We optimize models using the AdamW optimizer (Loshchilov and Hutter 2019) with a learning rate of  $4 \times 10^{-5}$  for aggregation layers. Training spans at most 80 epochs, with approximately 2000 iterations per epoch and a 4000-iteration linear learning rate warmup. A weight decay of  $1 \times 10^{-3}$  is applied. Clique Mining (CM) (Izquierdo and Civera 2024a) is used to group place data, with cliques being recomputed during training. The implementation is based on PyTorch Lightning, and the training is conducted on a single NVIDIA A100 GPU.

## Results

### Comparison with Baselines

In this section, we evaluate the R@1 performance of our proposed QAA method in comparison with state-of-the-art VPR methods. Results for multi-view datasets are presented in Table 2, while those for front-view datasets are shown in Table 3. Our comparison includes leading baselines such as NetVLAD (Arandjelovic et al. 2016), SRFS (Ge et al. 2020), Conv-AP (Ali-bey, Chaib-draa, and Giguère 2022), MixVPR (Ali-bey, Chaib-draa, and Giguère 2023), CosPlace (Berton, Masone, and Caputo 2022), EigenPlace (Berton et al. 2023), BoQ (Ali-bey,

Table 2: Recall@1 Comparison of state-of-the-art VPR methods with our results on large-scale multi-view VPR datasets. The best results are highlighted in **bold** and the rest of the top-3 results are underlined.

	Backbones	$C_d$	AmsterTime	Eynsham	Pitts250k	Pitts30k	SPED	SF-XL v1	SF-XL v2	Tokyo24/7
NetVLAD (Arandjelovic et al. 2016)	VGG-16	4096	16.3	77.7	85.9	85.0	-	40.0	76.9	69.8
SRFS (Ge et al. 2020)	VGG-16	4096	29.7	72.3	90.4	89.1	-	50.3	83.8	80.3
Conv-AP (Ali-bey, Chaib-draa, and Giguère 2022)	ResNet-50	4096	33.9	87.5	92.4	90.5	80.1	47.5	74.4	76.2
MixVPR (Ali-bey, Chaib-draa, and Giguère 2023)	ResNet-50	4096	40.2	89.4	94.2	91.5	85.2	71.1	88.5	85.1
CosPlace (Berton, Masone, and Caputo 2022)	ResNet-50	2048	47.7	90.0	92.3	90.9	75.3	76.4	88.8	87.3
EigenPlace (Berton et al. 2023)	ResNet-50	2048	48.9	90.7	94.1	92.5	82.4	84.1	90.8	93.0
BoQ (Ali-bey, Chaib-draa, and Giguère 2024)	DINOv2-B	12288	<u>63.0</u>	92.2	<b>96.6</b>	93.7	<b>92.5</b>	<u>91.8</u>	<b>95.2</b>	<u>98.1</u>
SALAD CM (Izquierdo and Civera 2024b,a)	DINOv2-B	8448	58.1	91.9	95.2	92.6	89.1	<u>85.6</u>	<u>94.6</u>	96.8
		8192	<b>63.7</b>	<b>92.9</b>	<b>96.6</b>	<b>94.4</b>	<u>91.8</u>	<b>94.4</b>	<u>94.6</u>	<b>98.4</b>
QAA (Ours)	DINOv2-B	4096	<u>61.8</u>	<u>92.9</u>	96.3	93.8	<u>91.1</u>	<u>94.2</u>	94.0	<u>97.8</u>
		2048	61.5	<u>92.7</u>	<u>96.4</u>	<u>94.0</u>	<u>91.1</u>	<u>94.0</u>	94.1	96.5
		1024	59.8	<u>92.5</u>	96.3	<u>93.9</u>	90.8	92.4	94.5	97.1

Table 3: Recall@1 Comparison of state-of-the-art VPR methods with our results on front-view VPR datasets. The best results are highlighted in **bold** and the rest of the top-3 results are underlined.

	Backbones	$C_d$	MSLS Val	MSLS Challenge	Nordland*	Nordland**	SVOX Night	SVOX Overcast	SVOX Rain	SVOX Snow	SVOX Sun
NetVLAD (Arandjelovic et al. 2016)	VGG-16	4096	58.9	-	-	13.1	8.0	66.4	51.5	54.4	35.4
SRFS (Ge et al. 2020)	VGG-16	4096	70.0	-	-	16.0	28.6	81.1	69.7	76.0	54.8
Conv-AP (Ali-bey, Chaib-draa, and Giguère 2022)	ResNet-50	4096	83.4	-	38.2	62.9	43.4	91.9	82.8	91.0	80.4
MixVPR (Ali-bey, Chaib-draa, and Giguère 2023)	ResNet-50	4096	88.0	64.0	58.4	76.2	64.4	96.2	91.5	96.8	84.8
CosPlace (Berton, Masone, and Caputo 2022)	ResNet-50	2048	87.4	67.5	54.4	71.9	50.7	92.2	87.0	92.0	78.5
EigenPlace (Berton et al. 2023)	ResNet-50	2048	89.2	67.4	54.2	71.2	58.9	93.1	90.0	93.1	86.4
BoQ (Ali-bey, Chaib-draa, and Giguère 2024)	DINOv2-B	12288	93.8	79.0	81.3	90.6	<b>97.7</b>	<b>98.5</b>	<b>98.8</b>	<b>99.4</b>	<u>97.5</u>
SALAD CM (Izquierdo and Civera 2024b,a)	DINOv2-B	8448	94.2	82.7	90.7	95.2	95.6	<b>98.5</b>	<u>98.4</u>	<u>99.2</u>	<u>98.1</u>
		8192	97.6	<b>85.7</b>	<b>91.8</b>	<b>96.7</b>	<u>97.2</u>	98.4	<u>98.4</u>	<u>99.1</u>	97.3
QAA (Ours)	DINOv2-B	4096	<b>98.1</b>	84.8	<u>91.6</u>	96.6	<u>97.2</u>	<b>98.5</b>	97.9	99.0	<b>98.2</b>
		2048	<u>97.8</u>	<u>84.2</u>	<u>91.4</u>	<u>95.6</u>	96.4	98.4	97.5	98.3	97.1
		1024	<u>97.7</u>	82.1	88.3	92.2	95.0	98.6	97.7	99.0	95.9

Chaib-draa, and Giguère 2024), and SALAD with Clique Mining (CM) (Izquierdo and Civera 2024b,a). These methods represent some of the most effective and widely recognized one-stage approaches in the field. Notably, recent baselines like BoQ and SALAD CM have demonstrated superior accuracy and efficiency than two-stage methods.

Tables 2 and 3 reveal distinct strengths for BoQ and SALAD CM on multi-view and front-view datasets, respectively, due to their specialized training. BoQ’s training on a multi-view dataset creates a bias for such data, while SALAD CM’s training on both, combined with a limited model capacity, leads to overfitting on front-view characteristics. Our QAA method addresses these limitations by efficiently enhancing information capacity and extensive joint training. This strategy enables QAA to learn more generalized representations that are effective across both multi-view and front-view datasets, demonstrating superior generalization capabilities compared to BoQ and SALAD CM.

Specifically, as presented in Table 2, the QAA method surpasses BoQ on the AmsterTime, Eynsham, Pitts30k, SF-XL v1, and Tokyo 24/7 datasets, which are multi-view in nature. On the Pitts250k, SPED, and SF-XL v2 datasets, QAA achieves performance comparable to BoQ despite utilizing a significantly smaller output dimension (8192 vs. 12288). The reduced output dimension not only indicates computational efficiency but also suggests that QAA captures essential features without the need for a larger output descriptor dimension. These results highlight the effectiveness of our method on multi-view datasets and underscore its competi-

tive advantage over state-of-the-art baselines.

Similarly, as shown in Table 3, QAA significantly outperforms both SALAD CM and BoQ on the MSLS and Nordland evaluation sets. It also achieves performance on par with SALAD CM and BoQ on the SVOX evaluation sets. Notably, despite SALAD CM’s training bias toward front-view datasets, our method delivers superior overall performance on front-view datasets. This demonstrates that QAA yields balanced and optimal performance to different dataset types, validating its robustness and adaptability.

**Performance of Reduced  $C_d$ .** Tables 2 and 3 present the performance of reduced  $C_d$ . For  $C_d = 4096$  and  $2048$ , QAA overall maintains strong performance, particularly on the Eynsham, Pitts250k, Pitts30k, SPED, SF-XL, Tokyo24/7, MSLS Val and Challenge, Nordland, and SVOX evaluation sets. A mild performance degradation is observed for  $C_d = 1024$  on AmsterTime, SF-XL v1, MSLS Challenge, Nordland, SVOX Night, and SVOX Sun, while performance remains competitive on other datasets. These results highlight the robustness of QAA.

**Inference Complexity.** We compare the computational and parameter complexity of DINOv2 SALAD, BoQ, and QAA. SALAD employs 1.4M parameters for its aggregation module and, for a  $322 \times 322$  image, requires 0.94 GFLOPS with convolution-based aggregation. For attention-based aggregation, BoQ, with 64 queries, utilizes 8.6M parameters and 8.22 GFLOPS. Compared with BoQ, QAA, despite using 256 queries, requires only 5.1M parameters and 2.29 GFLOPS while maintaining the reduced output size.

Table 4: Performance Comparison for Joint Training across Different Datasets with SALAD CM (Izquierdo and Civera 2024a) and Our QAA Approaches ( $N_q = 256, C_f = 64, C_r = 128, C_d = 8192$ ). All methods incorporate Clique Mining (CM) (Izquierdo and Civera 2024a) and DINOv2-B backbone. The best results are highlighted in **bold**.

Training Datasets	Methods	MSLS Val	Pitts250k Val	SF-XL Val	Nordland*	AmsterTime
GSV-Cities	SALAD CM	<b>92.7</b>	94.4	93.8	<b>70.9</b>	58.6
	QAA	<b>92.7</b>	<b>95.0</b>	<b>95.2</b>	69.5	<b>64.6</b>
MSLS	SALAD CM	97.6	92.2	90.8	88.7	48.5
	QAA	<b>98.1</b>	<b>93.2</b>	<b>92.7</b>	<b>89.5</b>	<b>53.7</b>
SF-XL	SALAD CM	<b>94.2</b>	95.1	94.2	87.4	59.6
	QAA	93.8	<b>95.5</b>	<b>97.0</b>	<b>88.6</b>	<b>61.7</b>
GSV-Cities + MSLS + SF-XL	SALAD CM	96.6	95.1	97.0	90.3	60.6
	QAA	<b>97.6</b>	<b>95.4</b>	<b>97.8</b>	<b>91.8</b>	<b>63.7</b>

Table 5: Performance Comparison for Joint Training across Different Settings for Aggregation Methods with Independent Reference Codebooks. The best results are in **bold**.

Methods	MSLS Val	Pitts250k Val	SF-XL Val	Nordland*	AmsterTime
Softmax	97.0	94.9	97.7	90.5	61.5
OT	97.3	95.3	97.5	90.9	62.0
CS	<b>97.6</b>	<b>95.4</b>	<b>97.8</b>	<b>91.8</b>	<b>63.7</b>

Table 6: Performance Comparison for Joint Training across Different Numbers of Queries  $N_q$  with  $C_f = 64$  and  $C_r = 128$ . The best results are highlighted in **bold**. For inference complexity, GFLOPS is computed for the QAA module using a single  $322 \times 322$  image.

$N_q$	GFLOPS	MSLS Val	Pitts250k Val	SF-XL Val	Nordland*	AmsterTime
16	1.31	<b>97.6</b>	95.1	96.4	88.3	59.2
32	1.38	<b>97.6</b>	95.3	97.1	89.6	61.6
64	1.51	<b>97.6</b>	95.2	97.7	91.1	60.6
128	1.77	<b>97.6</b>	<b>95.4</b>	<b>97.8</b>	<b>92.8</b>	63.5
256	2.29	<b>97.6</b>	<b>95.4</b>	<b>97.8</b>	91.8	<b>63.7</b>

## Ablation Study

We evaluate the effectiveness and examine the underlying mechanism of our QAA approach, aiming to achieve balanced and optimal performance across a wide range of datasets. We assess validation R@1 performance on MSLS, Pitts250, and SF-XL, as their performance is closely tied to the training datasets. To evaluate generalization performance across markedly different data attributes, we include the Nordland\* and AmsterTime datasets in our study. These datasets introduce significant domain variations, such as seasonal transitions from summer to winter and the presence of historical grayscale images.

**Cross-Dataset Evaluation.** Table 4 presents the cross-dataset evaluation results using the DINOv2 SALAD CM approach (Izquierdo and Civera 2024a) and our QAA approaches. The findings reveal that models trained on individual datasets achieve the highest accuracy on their respective evaluation sets but struggle on others, indicating an inductive bias toward the specific characteristics of the training data. In contrast, joint training on GSV-Cities, MSLS, and SF-XL leads to more balanced performance across all three validation sets, as well as on significantly different datasets such as Nordland and AmsterTime. However, joint training neg-

atively impacted MSLS Val performance on SALAD CM, though QAA still performed comparably to models trained exclusively on MSLS. Moreover, our QAA approaches consistently outperform the SALAD CM method across various training configurations, with particularly strong improvements on MSLS Val, SF-XL Val, Nordland, and AmsterTime, underscoring QAA’s superior accuracy.

**Effectiveness of Independent Reference Codebooks and CS Matrix.** Table 5 presents a performance comparison of QAA under different aggregation paradigms: (1) Softmax, (2) Optimal Transportation (OT), and (3) Cross-query Similarity (CS). The results highlight two key observations: (1) the efficacy of using an independent reference codebook across different paradigms, and (2) the superior performance of CS, particularly on the MSLS Val, Nordland, and AmsterTime datasets, emphasizing the advantage of similarity-based aggregation in enhancing VPR representations.

**Coding Rate Analysis.** We analyze the information capacity of  $\hat{P}$  by examining the histogram of coding rates per query using the MSLS Val in Fig. 4. The results indicate that  $\hat{P}$  generated by CS exhibits a  $\sim 2\times$  coding rate with reduced variance compared to Softmax and OT, both of which compress the output space and restrict information content. In contrast, CS preserves more information in query-level image features, enabling richer interactions with the reference codebook. This enhanced information retention facilitates the generation of highly informative descriptors, ultimately leading to superior performance.

**Query Scalability.** Table 6 explores the relationship between the number of queries,  $N_q$ , and the performance of QAA. The results indicate that increasing  $N_q$  enhances QAA’s performance on Pitts250k, SF-XL Val, Nordland, and AmsterTime, with performance gains saturating at  $N_q = 128$  and  $N_q = 256$ . The MSLS Val performance remains stable across different  $N_q$ , indicating that this evaluation set follows a consistent pattern from the fixed front-viewpoint. Therefore, fewer queries are required to capture the pattern effectively. This highlights the importance of a larger  $N_q$  in optimizing QAA’s effectiveness.

**Effect of Channel Numbers.** Table 7 analyzes performance variations across different values of  $C_f$  and  $C_r$ , which influence the final output dimension  $C_d$ . We observe

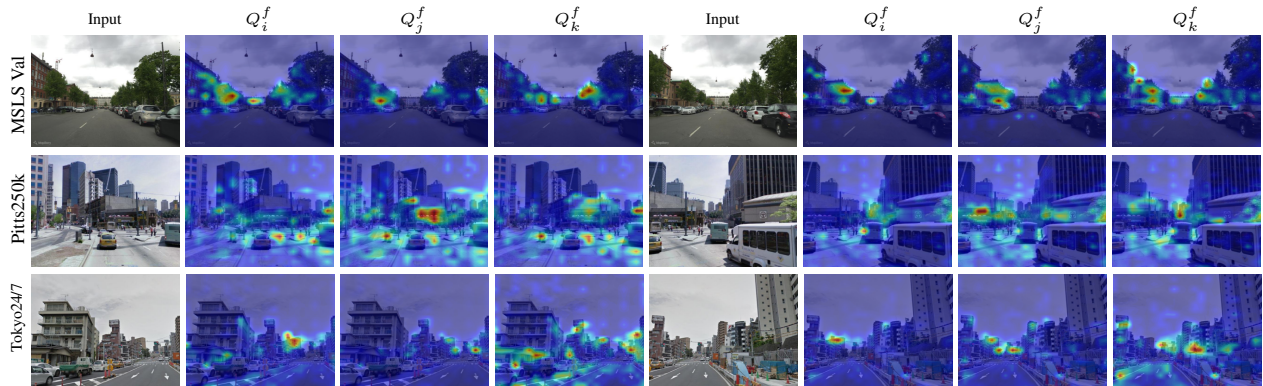


Figure 3: Attention Maps Corresponding to Different Query Vectors ( $Q_i^f$ ,  $Q_j^f$ , and  $Q_k^f$ ) in  $Q^f$  from The Feature Prediction Model for A Front-view Dataset (MSLS Val) and Multi-view Datasets (Pitts250k and Tokyo24/7). Each pair of images represents the same location within the same dataset but from different viewpoints.

Table 7: Performance Comparison for Joint Training across Different Numbers of Channels for Learned Queries  $C_f$  and  $C_r$  with  $N_q = 256$ . The best results are highlighted in **bold**.

$C_f$	$C_r$	$C_d$	MSLS Val	Pitts250k Val	SF-XL Val	Nordland*	AmsterTime
64	128	8192	97.6	95.4	97.8	91.8	63.7
64	64	4096	97.7	95.4	97.4	91.0	<b>63.0</b>
32	128	4096	<b>98.1</b>	<b>95.5</b>	<b>97.7</b>	<b>91.6</b>	61.8
64	32	2048	97.4	<b>95.2</b>	<b>97.2</b>	90.4	<b>61.5</b>
16	128	2048	<b>97.8</b>	95.0	97.0	<b>91.4</b>	<b>61.5</b>
64	16	1024	<b>97.7</b>	<b>95.2</b>	<b>96.3</b>	<b>89.3</b>	58.9
8	128	1024	<b>97.7</b>	95.1	96.0	88.3	<b>59.8</b>

that reducing either  $C_f$  or  $C_r$  results in a slight but comparable performance degradation. Interestingly, the model remains robust **even when  $C_f$  is extremely reduced to 8**, despite the information bottleneck in the query-level image feature  $\hat{P}$ , whose dimension shrinks to  $256 \times 8$ . This resilience is attributed to the support of the high-dimensional codebook  $\hat{F}$ , which helps maintain performance stability.

### Qualitative Results

Figure 3 presents attention maps corresponding to different vectors in  $Q^f$  for the feature prediction model, evaluated across the MSLs Val, Pitts250k, and Tokyo24/7 datasets:

- **Global Context Capture:** The multi-attention module allows attention maps to span the entire image, capturing global context rather than relying solely on patch-level feature combinations. This broader perspective likely contributes to the performance gains in experiments.
- **Diverse Attention Patterns:** Different query vectors exhibit unique attention patterns. For instance, some queries focus on distant objects in the foreground, while others emphasize nearby roads or structures. This diversity in attention may further enhance model performance.
- **Consistency Across Viewpoints:** Each pair of attention maps for the same location, taken from different viewpoints, highlights similar landmarks, while the overall patterns adjust based on the changes in viewpoint.

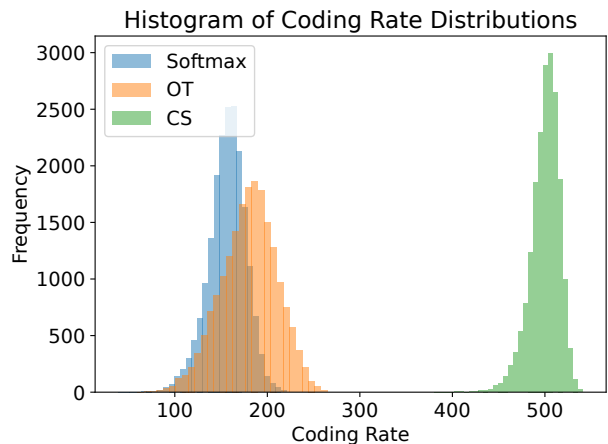


Figure 4: Histogram of the coding rate distributions for different aggregation paradigms.

### Conclusions

This work introduces the Query-based Adaptive Aggregation (QAA) method with the Cross-query Similarity (CS) paradigm for enhancing VPR multi-dataset training performance. Extensive evaluations demonstrate that QAA consistently achieves high performance across diverse evaluation datasets, excelling in: (1) capturing global context for query-level image features and independent reference codebooks, (2) handling scalable queries without increasing output dimensionality, and (3) enabling efficient query training with minimal computational and parameter overhead. Moreover, we demonstrate for the first time that the CS matrix, with better informational capacity than score-based aggregation, can generate robust geographical descriptors for VPR. These findings further highlight the broad potential of QAA and the CS matrix for tasks requiring enhanced information capacity or robust feature representations. Future work will address the challenge of performance saturation when  $N_q$  is large.

## References

- Ali-bey, A.; Chaib-draa, B.; and Giguère, P. 2022. GSV-Cities: Toward appropriate supervised visual place recognition. *Neurocomputing*, 513: 194–203.
- Ali-bey, A.; Chaib-draa, B.; and Giguère, P. 2023. MixVPR: Feature Mixing for Visual Place Recognition. In *Proceedings of the IEEE/CVF Winter Conference on Applications of Computer Vision*, 2998–3007.
- Ali-bey, A.; Chaib-draa, B.; and Giguère, P. 2024. BoQ: A Place is Worth a Bag of Learnable Queries. In *Proceedings of the IEEE/CVF Conference on Computer Vision and Pattern Recognition (CVPR)*, 17794–17803.
- Arandjelovic, R.; Gronat, P.; Torii, A.; Pajdla, T.; and Sivic, J. 2016. NetVLAD: CNN architecture for weakly supervised place recognition. In *Proceedings of the IEEE conference on computer vision and pattern recognition*, 5297–5307.
- Berton, G.; and Masone, C. 2025. MegaLoc: One Retrieval to Place Them All. In *Proceedings of the Computer Vision and Pattern Recognition Conference (CVPR) Workshops*, 2861–2867.
- Berton, G.; Masone, C.; and Caputo, B. 2022. Rethinking Visual Geo-Localization for Large-Scale Applications. In *Proceedings of the IEEE/CVF Conference on Computer Vision and Pattern Recognition (CVPR)*, 4878–4888.
- Berton, G.; Mereu, R.; Trivigno, G.; Masone, C.; Csurka, G.; Sattler, T.; and Caputo, B. 2022. Deep visual geo-localization benchmark. In *Proceedings of the IEEE/CVF Conference on Computer Vision and Pattern Recognition*, 5396–5407.
- Berton, G.; Trivigno, G.; Caputo, B.; and Masone, C. 2023. EigenPlaces: Training Viewpoint Robust Models for Visual Place Recognition. In *Proceedings of the IEEE/CVF International Conference on Computer Vision (ICCV)*, 11080–11090.
- Berton, G. M.; Paolicelli, V.; Masone, C.; and Caputo, B. 2021. Adaptive-Attentive Geolocalization From Few Queries: A Hybrid Approach. In *Proceedings of the IEEE/CVF Winter Conference on Applications of Computer Vision (WACV)*, 2918–2927.
- Campos, C.; Elvira, R.; Rodríguez, J. J. G.; M. Montiel, J. M.; and D. Tardós, J. 2021. ORB-SLAM3: An Accurate Open-Source Library for Visual, Visual-Inertial, and Multimap SLAM. *IEEE Transactions on Robotics*, 37(6): 1874–1890.
- Chen, Z.; Jacobson, A.; Sünderhauf, N.; Upcroft, B.; Liu, L.; Shen, C.; Reid, I.; and Milford, M. 2017. Deep learning features at scale for visual place recognition. In *2017 IEEE International Conference on Robotics and Automation (ICRA)*, 3223–3230.
- Couturier, A.; and Akhloufi, M. A. 2021. A review on absolute visual localization for UAV. *Robotics and Autonomous Systems*, 135: 103666.
- Cummins, M. J.; and Newman, P. 2009. Highly scalable appearance-only SLAM - FAB-MAP 2.0. In *Robotics: Science and Systems*.
- Cuturi, M. 2013. Sinkhorn distances: Lightspeed computation of optimal transport. *Advances in neural information processing systems*, 26.
- Dosovitskiy, A.; Beyer, L.; Kolesnikov, A.; Weissenborn, D.; Zhai, X.; Unterthiner, T.; Dehghani, M.; Minderer, M.; Heigold, G.; Gelly, S.; Uszkoreit, J.; and Hounsby, N. 2021. An Image is Worth 16x16 Words: Transformers for Image Recognition at Scale. In *International Conference on Learning Representations*.
- Ge, Y.; Wang, H.; Zhu, F.; Zhao, R.; and Li, H. 2020. Self-supervising fine-grained region similarities for large-scale image localization. In *Computer Vision—ECCV 2020: 16th European Conference, Glasgow, UK, August 23–28, 2020, Proceedings, Part IV 16*, 369–386. Springer.
- Izquierdo, S.; and Civera, J. 2024a. Close, But Not There: Boosting Geographic Distance Sensitivity in Visual Place Recognition. *arXiv preprint arXiv:2407.02422*.
- Izquierdo, S.; and Civera, J. 2024b. Optimal Transport Aggregation for Visual Place Recognition. In *Proceedings of the IEEE/CVF Conference on Computer Vision and Pattern Recognition (CVPR)*.
- Keetha, N.; Mishra, A.; Karhade, J.; Jatavallabhula, K. M.; Scherer, S.; Krishna, M.; and Garg, S. 2023. Anyloc: Towards universal visual place recognition. *IEEE Robotics and Automation Letters*.
- LeCun, Y.; Bengio, Y.; and Hinton, G. 2015. Deep learning. *nature*, 521(7553): 436–444.
- Leyva-Vallina, M.; Strisciuglio, N.; and Petkov, N. 2023. Data-efficient large scale place recognition with graded similarity supervision. In *Proceedings of the IEEE/CVF Conference on Computer Vision and Pattern Recognition*, 23487–23496.
- Liu, B.; Zhang, P.; He, L.; Chen, H.; Guo, S.; Wu, Y.; Cui, J.; and Zhang, H. 2025. SuperPlace: The Renaissance of Classical Feature Aggregation for Visual Place Recognition in the Era of Foundation Models. *arXiv preprint arXiv:2506.13073*.
- Loshchilov, I.; and Hutter, F. 2019. Decoupled Weight Decay Regularization. In *International Conference on Learning Representations*.
- Lu, F.; Zhang, L.; Lan, X.; Dong, S.; Wang, Y.; and Yuan, C. 2024. Towards Seamless Adaptation of Pre-trained Models for Visual Place Recognition. In *The Twelfth International Conference on Learning Representations*.
- Ma, Y.; Derksen, H.; Hong, W.; and Wright, J. 2007. Segmentation of multivariate mixed data via lossy data coding and compression. *IEEE transactions on pattern analysis and machine intelligence*, 29(9): 1546–1562.
- Masone, C.; and Caputo, B. 2021. A Survey on Deep Visual Place Recognition. *IEEE Access*, 9: 19516–19547.
- Oquab, M.; Darcet, T.; Moutakanni, T.; Vo, H. V.; Szafraniec, M.; Khalidov, V.; Fernandez, P.; HAZIZA, D.; Massa, F.; El-Nouby, A.; Assran, M.; Ballas, N.; Galuba, W.; Howes, R.; Huang, P.-Y.; Li, S.-W.; Misra, I.; Rabbat, M.; Sharma, V.; Synnaeve, G.; Xu, H.; Jegou, H.; Mairal,

- J.; Labatut, P.; Joulin, A.; and Bojanowski, P. 2024. DI-NOv2: Learning Robust Visual Features without Supervision. *Transactions on Machine Learning Research*.
- Sarlin, P.-E.; Cadena, C.; Siegwart, R.; and Dymczyk, M. 2019. From coarse to fine: Robust hierarchical localization at large scale. In *Proceedings of the IEEE/CVF conference on computer vision and pattern recognition*, 12716–12725.
- Schubert, S.; Neubert, P.; Garg, S.; Milford, M.; and Fischer, T. 2024. Visual Place Recognition: A Tutorial [Tutorial]. *IEEE Robotics & Automation Magazine*, 31(3): 139–153.
- Sinkhorn, R.; and Knopp, P. 1967. Concerning nonnegative matrices and doubly stochastic matrices. *Pacific Journal of Mathematics*, 21(2): 343–348.
- Sünderhauf, N.; Neubert, P.; and Protzel, P. 2013. Are we there yet? Challenging SeqSLAM on a 3000 km journey across all four seasons. In *Proc. of workshop on long-term autonomy, IEEE international conference on robotics and automation (ICRA)*, 2013.
- Torii, A.; Arandjelović, R.; Sivic, J.; Okutomi, M.; and Pajdla, T. 2015. 24/7 place recognition by view synthesis. In *2015 IEEE Conference on Computer Vision and Pattern Recognition (CVPR)*, 1808–1817.
- Torii, A.; Sivic, J.; Pajdla, T.; and Okutomi, M. 2013. Visual place recognition with repetitive structures. In *Proceedings of the IEEE conference on computer vision and pattern recognition*, 883–890.
- Trivigno, G.; Berton, G.; Aragon, J.; Caputo, B.; and Masone, C. 2023. Divide&Classify: Fine-Grained Classification for City-Wide Visual Geo-Localization. In *Proceedings of the IEEE/CVF International Conference on Computer Vision (ICCV)*, 11142–11152.
- Tzachor, I.; Lerner, B.; Levy, M.; Green, M.; Shalev, T. B.; Habib, G.; Samuel, D.; Zailer, N. K.; Shimshi, O.; Darshan, N.; and Ben-Ari, R. 2025. EffoVPR: Effective Foundation Model Utilization for Visual Place Recognition. In *The Thirteenth International Conference on Learning Representations*.
- Vaswani, A.; Shazeer, N.; Parmar, N.; Uszkoreit, J.; Jones, L.; Gomez, A. N.; Kaiser, Ł.; and Polosukhin, I. 2017. Attention is all you need. *Advances in neural information processing systems*, 30.
- Wang, R.; Shen, Y.; Zuo, W.; Zhou, S.; and Zheng, N. 2022. TransVPR: Transformer-Based Place Recognition With Multi-Level Attention Aggregation. In *Proceedings of the IEEE/CVF Conference on Computer Vision and Pattern Recognition (CVPR)*, 13648–13657.
- Wang, X.; Han, X.; Huang, W.; Dong, D.; and Scott, M. R. 2019. Multi-similarity loss with general pair weighting for deep metric learning. In *Proceedings of the IEEE/CVF conference on computer vision and pattern recognition*, 5022–5030.
- Warburg, F.; Hauberg, S.; López-Antequera, M.; Gargallo, P.; Kuang, Y.; and Civera, J. 2020. Mapillary Street-Level Sequences: A Dataset for Lifelong Place Recognition. In *2020 IEEE/CVF Conference on Computer Vision and Pattern Recognition (CVPR)*, 2623–2632.
- Xiao, J.; Tortei, D.; Roura, E.; and Loianno, G. 2023. Long-Range UAV Thermal Geo-Localization with Satellite Imagery. In *2023 IEEE/RSJ International Conference on Intelligent Robots and Systems (IROS)*, 5820–5827.
- Xiao, J.; Zhu, G.; and Loianno, G. 2025. VG-SSL: Benchmarking Self-Supervised Representation Learning Approaches for Visual Geo-Localization. In *Proceedings of the Winter Conference on Applications of Computer Vision (WACV)*, 6667–6677.
- Yildiz, B.; Khademi, S.; Siebes, R. M.; and Van Gemert, J. 2022. Amstertime: A visual place recognition benchmark dataset for severe domain shift. In *2022 26th International Conference on Pattern Recognition (ICPR)*, 2749–2755. IEEE.
- Yu, Y.; Chan, K. H. R.; You, C.; Song, C.; and Ma, Y. 2020. Learning Diverse and Discriminative Representations via the Principle of Maximal Coding Rate Reduction. In Larochelle, H.; Ranzato, M.; Hadsell, R.; Balcan, M.; and Lin, H., eds., *Advances in Neural Information Processing Systems*, volume 33, 9422–9434. Curran Associates, Inc.
- Zaffar, M.; Garg, S.; Milford, M.; Kooij, J.; Flynn, D.; McDonald-Maier, K.; and Ehsan, S. 2021. Vpr-bench: An open-source visual place recognition evaluation framework with quantifiable viewpoint and appearance change. *International Journal of Computer Vision*, 129(7): 2136–2174.
- Zhu, S.; Yang, L.; Chen, C.; Shah, M.; Shen, X.; and Wang, H. 2023. R2Former: Unified Retrieval and Reranking Transformer for Place Recognition. In *Proceedings of the IEEE/CVF Conference on Computer Vision and Pattern Recognition (CVPR)*, 19370–19380.